Solar Physics (2021) 296:116
https://doi.org/10.1007/s11207-021-01861-x

Active Region Contributions to the Solar Wind over Multiple Solar Cycles

David Stansby[1] · Lucie M. Green[1] · Lidia van Driel-Gesztelyi[1,2,3] · Timothy S. Horbury[4]

Received: 9 April 2021 / Accepted: 9 July 2021 / Published online: 6 August 2021
© The Author(s) 2021

Abstract
Both coronal holes and active regions are source regions of the solar wind. The distribution of these coronal structures across both space and time is well known, but it is unclear how much each source contributes to the solar wind. In this study we use photospheric magnetic field maps observed over the past four solar cycles to estimate what fraction of magnetic open solar flux is rooted in active regions, a proxy for the fraction of all solar wind originating in active regions. We find that the fractional contribution of active regions to the solar wind varies between 30% to 80% at any one time during solar maximum and is negligible at solar minimum, showing a strong correlation with sunspot number. While active regions are typically confined to latitudes $\pm 30^\circ$ in the corona, the solar wind they produce can reach latitudes up to $\pm 60^\circ$. Their fractional contribution to the solar wind also correlates with coronal mass ejection rate, and is highly variable, changing by $\pm 20\%$ on monthly timescales within individual solar maxima. We speculate that these variations could be driven by coronal mass ejections causing reconfigurations of the coronal magnetic field on sub-monthly timescales.

Keywords Solar cycle · Solar wind · Active regions · Coronal holes

1. Introduction

The solar wind is a flow of hot tenuous plasma, driven by the large pressure difference between the Sun's corona and the interplanetary medium. Not all areas of the corona escape to form the solar wind: in some areas plasma is confined on closed field lines, whereas in others the plasma accelerates until it becomes super-sonic and super-Alfvénic, carrying magnetic flux out into interplanetary space to form the solar wind.

✉ D. Stansby
d.stansby@ucl.ac.uk

1 Mullard Space Science Laboratory, University College London, Holmbury St. Mary, Surrey, RH5 6NT, UK

2 LESIA, Observatoire de Paris, Université PSL, CNRS, Sorbonne Université, Université Paris Diderot, Sorbonne Paris Cité, 92195 Meudon, France

3 Konkoly Observatory, Research Centre for Astronomy and Earth Sciences, Konkoly Thege u. 15-17, 1121, Budapest, Hungary

4 Imperial College London, South Kensington Campus, London, SW7 2AZ, UK

The global properties of the solar wind vary with, and are ultimately controlled by, the Sun's 11 year activity cycle (e.g. McComas et al., 2013). At the beginning of a cycle, during solar minima, the corona is dominated by two polar coronal holes at high latitudes. These host open magnetic field lines, while at low latitudes closed loops dominate. This relatively simple configuration is disrupted by strong concentrations of magnetic flux emerging through the photosphere at low latitudes, forming new active regions (ARs, van Driel-Gesztelyi and Green, 2015; Cheung et al., 2017). As magnetic flux emerges through the photosphere it starts out closed, but as the field strength increases the closed loops can reconnect with adjacent open field lines (van Driel-Gesztelyi et al., 2014; Ma et al., 2014; Kong et al., 2018), redistributing regions of existing open flux (Sheeley, Wang, and Harvey, 1989; Baker, van Driel-Gesztelyi, and Attrill, 2007) and in the process opening up previously closed flux (Wang and Sheeley, 2003a; Attrill et al., 2006). This allows plasma originating in active regions to flow out from the corona and form part of the solar wind.

As time passes, photospheric footpoints of open field lines are subject to diffusion processes, causing the initially high concentrations of magnetic flux to spread out and become weaker (Leighton, 1964). As the magnetic field strength weakens these areas remain open and turn into low latitude equatorial coronal holes (Wang et al., 2010; Petrie and Haislmaier, 2013; Wang, 2017; Golubeva and Mordvinov, 2017). As the solar cycle progresses, the dominant polarity of each polar coronal hole is eroded, and new polar coronal holes of opposite polarity form. Eventually the rate of flux emergence at low latitudes decreases, leaving these two new polar coronal holes and marking the beginning of the subsequent cycle.

The idea that active regions could be source regions for solar wind was initially developed via global coronal models. These models predict where open flux is rooted, and in several individual cases predicted significant amounts of open flux rooted in active regions (Neugebauer et al., 2002; Wang and Sheeley, 2003b). This was subsequently backed up by evidence showing persistent upflows of coronal plasma on the edges of active regions (see Tian et al., 2021, for a review). Estimates of heavy ion composition within active regions match measurements in the solar wind, providing further evidence for active region contributions to the solar wind (Macneil et al., 2019; Stansby et al., 2020a).

While the spatial and temporal distribution of active regions has been known for a long time, how this translates into contributions to the solar wind is less well known. Schrijver and De Rosa (2003) used global coronal potential field source surface models to show an increase in the fraction of open flux rooted in active regions during the rising phase of Cycle 23, peaking at $\sim$30% during solar maximum (their Figure 11). Using a slightly different method, and considering only solar wind in the ecliptic plane Fu et al. (2015) concluded that ARs were the major contributor to solar wind measured at Earth during the maximum of Cycle 23, with the contribution declining from $\sim$60% to $\sim$10% during the declining phase of that cycle.

It is not clear whether these results are dependent on magnetogram data source (both Schrijver and De Rosa (2003) and Fu et al. (2015) only used a single source), and how the variation extends over multiple solar cycles. In this paper we perform such an analysis of active region solar wind sources, using four different magnetogram sources, allowing us to span the last four solar cycles, and check that different data sources agree when they overlap.

In Section 2 the data and methods used to distinguish between active region and coronal hole sources are explained. Results are presented in Section 3, showing that the fractional contribution of active regions to the solar wind can be up to 80% during solar maximum, showing a strong correlation with sunspot number. These results are placed in context and discussed in Section 4, with conclusions given in Section 5.

Table 1 Details of the data sources used in this study. Text in the "Data" column are clickable http or ftp links.

Observatory	Date range	AR threshold (G)	Data
KPVT	1975 Feb. 19 – 2003 Aug. 29	35	Link
MDI	1996 Jun. 28 – 2010 Nov. 26	100	Link
SOLIS	2003 Aug. 16 – 2017 Oct. 23	40	Link
GONG	2006 Oct. 18 – 2021 Apr. 14	30	Link

2. Methods

Because both the heliospheric magnetic flux and solar wind mass flux are approximately independent of latitude and longitude in the heliosphere (Lockwood and Owens, 2009; Wang, 2010; McComas et al., 2013), measuring the fraction of open magnetic flux rooted within different coronal source regions is a convenient proxy for the amount of solar wind originating in different source regions. In the following subsections we give an overview of how the photospheric footpoints of open flux were computed (Section 2.1) and how coronal hole and active region areas were distinguished (Section 2.2).

2.1. PFSS Modeling

To estimate where open flux is rooted in the photosphere, potential field source surface (PFSS, Altschuler and Newkirk, 1969; Schatten, Wilcox, and Ness, 1969) modeling was carried out using the `pfsspy` software package (Stansby, Yeates, and Badman, 2020). Several observatories provide synoptic magnetic field maps, using different observing equipment, techniques, and data processing pipelines (see e.g. Riley et al., 2014, Table 1 for a list). In this study synoptic maps from the Kitt Peak Vacuum Telescope (KPVT, Livingston et al., 1976), Michelson Doppler Interferometer (MDI, Scherrer et al., 1995), Synoptic Optical Long-term Investigations of the Sun (SOLIS, Keller and NSO Staff, 1998), and Global Oscillations Network Group (GONG, Harvey et al., 1996) were used. Between them these data sources provide synoptic maps of the radial component of magnetic field in the photosphere, spanning more than four solar cycles at a rate of one map per Carrington rotation. KPVT, SOLIS, and GONG maps are provided at a native resolution of 360 × 180 (longitude × sin latitude), and MDI maps were re-binned from 3600 × 1080 to this lower resolution. Table 1 lists the data products along with their temporal coverage and links to the data.

PFSS solutions for individual magnetograms were calculated on a 360 × 180 grid in (longitude × sin latitude) and 50 grid points in the radial direction between the solar surface ($R_\odot$) and source surface (R_{ss}). Magnetic field lines were then traced from an evenly spaced 360 × 180 grid at R_{ss} down to $R_\odot$. For each individual field line this resulted in six quantities: the source surface latitude and longitude from which the field line was traced (θ_{ss}, ϕ_{ss}), the solar surface footpoint latitude and longitude ($\theta_\odot, \phi_\odot$), and the radial magnetic field strength, both on the source and solar surfaces ($B_{r,ss}$, $B_{r,\odot}$). The resulting dataset is available at DOI, and the code used to generate it at DOI.

Two examples of this methodology are shown in Figure 1, one during solar minimum (left hand panels) and one during solar maximum (right hand panels). The top two panels show the photospheric maps used as input to the PFSS modeling, and the middle two panels show the photospheric footpoints of open field lines, colored by $B_{r,\odot}$. The bottom panels show the partitioning of open field lines into active region and coronal hole regions; for more details see Section 2.2.

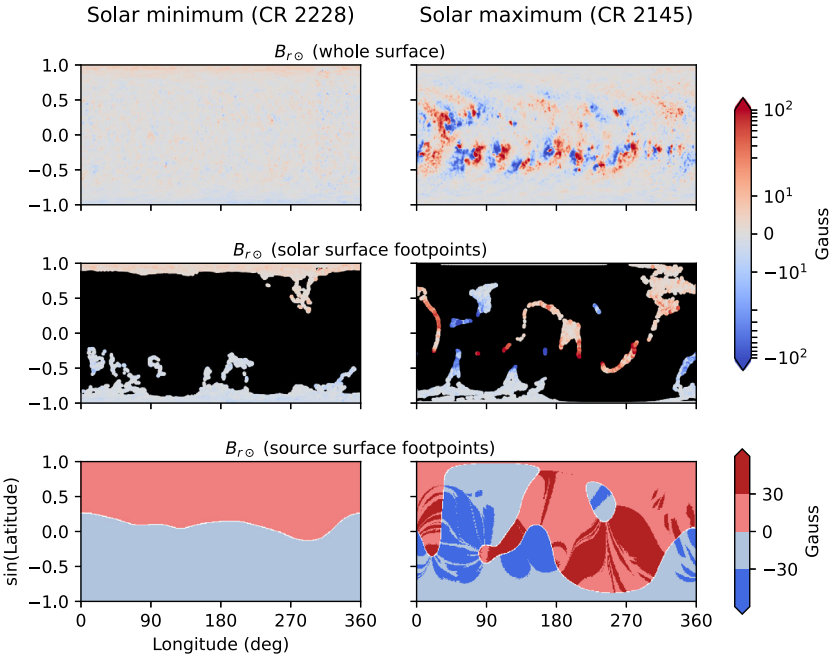

Figure 1 Photospheric magnetic field maps and open field regions at a solar minimum (left column) and a solar maximum (right column). Top rows show the photospheric magnetic field map. Middle rows show the open field footpoints from field lines traced down from an equal area grid at the source surface. The points are colored by their photospheric magnetic field polarity and strength. The bottom row shows categorization of source surface magnetic field lines into coronal hole (light colors) and active region (dark colors) sources. Both input magnetograms are from GONG.

2.1.1. Choice of Source Surface Height

The source surface height (R_{ss}) is a parameter of PFSS models that must be chosen to calculate a solution. Various methods can been used to choose an optimal source surface height, where optimal is defined relative to a given observational signature. Examples include matching total unsigned open flux to that measured in-situ in the solar wind (e.g. Lee et al., 2011; Arden, Norton, and Sun, 2014; Virtanen, Koskela, and Mursula, 2020), matching heliospheric current sheet crossings to those measured in-situ (e.g. Hoeksema, Wilcox, and Scherrer, 1983; Badman et al., 2020), or matching the locations of large open field regions with observations of coronal holes in extreme ultra-violet (EUV) images (e.g. Asvestari et al., 2019). 'Optimal' source surface heights vary between methods and location within the solar cycle, but R_{ss} almost always lies somewhere in the range $[1.5, 3.0]\ R_\odot$.

To test the robustness of our results against changes in R_{ss}, all analysis was run for four source surface heights, $R_{ss} = \{1.5, 2.0, 2.5, 3.0\}\ R_\odot$. The key quantitive result of this paper is not significantly affected by changes in the source surface height (demonstrated later in the Appendix), so for simplicity all results in the main body are shown for $R_{ss} = 2.0\ R_\odot$. We have inspected a full set of figures from the analysis run at each height to confirm that qualitative conclusions do not change either.

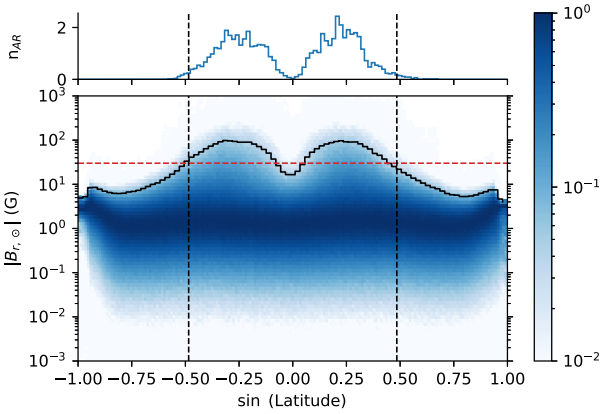

Figure 2 Distribution of photospheric radial magnetic field strength as a function of latitude from GONG synoptic maps. The data are a complete set of GONG maps from 8 January 2007 – 25 December 2020 sampled once per Carrington rotation. Solid black line shows the 99th percentile of magnetic field values. The top panel shows the distribution of NOAA active region latitudes for the same time period. Vertical dashed lines denote the 1st and 99th percentile of AR latitudes. The red horizontal line is drawn at 30 G, the threshold chosen to separate coronal hole and active region areas for GONG.

2.2. Distinguishing Coronal Holes and Active Regions

A key observational difference between coronal holes and active regions is their photospheric magnetic field strength. Coronal holes contain weak fields, compared to active regions with much stronger fields. This makes it possible to set a threshold below which a photospheric footpoint is considered rooted in a coronal hole, and above which it is rooted in an active region.

To aid in choosing such a threshold, Figure 2 shows the distribution of open footpoint field strengths as a function of latitude for all GONG magnetograms used here. As expected the strongest fields occur at mid-latitudes, where active regions are present. To confirm this, the top panel of Figure 2 shows the distribution of NOAA active region latitudes during the interval spanned by the magnetic field maps, with the 1st and 99th percentile AR latitudes indicated with vertical dashed black lines.

Outside active region latitudes, it is assumed that all open field footpoints fall within coronal holes. A lower limit on active region magnetic field strength can therefore be set as the maximum field strength outside active region latitudes. Figure 2 demonstrates how this threshold was chosen for GONG. Tracing the 1st and 99th percentile of AR latitudes down to distributions of magnetic field strength, and then finding the intersection with the 99th percentile or $B_{r,\odot}$ at these latitudes gives a threshold of 30 G, as indicated by the horizontal red line. Because the magnitude of magnetic fields measured by different observatories are systematically different (Riley et al., 2014; Virtanen and Mursula, 2017), this threshold identification process was repeated for each magnetogram source, with the thresholds reported in Table 1. These thresholds are all above published estimates for noise levels, which are around 5 G for MDI (Liu et al., 2012), 5 G for KPVT (Wenzler et al., 2004), 1 G for SOLIS (Harvey et al., 2003), and 3 G for GONG (Clark et al., 2003).

While these thresholds may seem low for an active region, they are averaged over a 1 deg^2 area of the photosphere, washing out the peak values present at smaller scales. In addition, the thresholds used here are similar to thresholds used for assimilating newly observed active

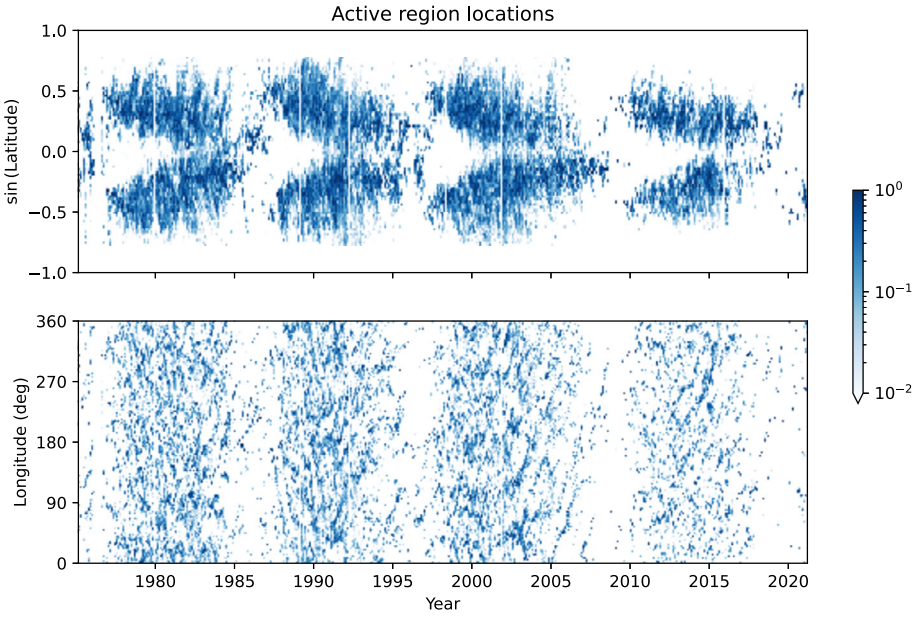

Figure 3 Distribution of open field solar surface footpoints in active regions as a function of time, column normalized. The top panel shows distributions in sin(latitude) (summed over all longitudes), and the bottom panel distributions in longitude (summed over all latitudes). Full datasets are used from KPVT and GONG, with the gap between filled by MDI.

regions in the literature, which variously are 15 G (Yeates, Baker, and van Driel-Gesztelyi, 2015), 40 G (Whitbread et al., 2017), and 50 G (Virtanen et al., 2017).

As well as separating by magnetic field strength, it is also necessary to impose a threshold on the latitude of open field footpoints. Measurements of $B_{r,\odot}$ at the poles of the Sun are either un-obtainable due to the small tilt between the ecliptic plane and solar equator, and even when possible are challenging to measure, as only the line-of-sight (i.e. not radial) component can be directly observed. Because of these issues, the makers of synoptic maps must extrapolate values to fill in the polar regions. Different observatories use different methods, some of which result in large magnetic field values at the poles, which a simple threshold on $|B_r|$ would incorrectly identify as active region open field. Because (to our knowledge) no active regions have been observed at the poles of the Sun, we make the further assumption that any open field rooted at latitudes above $\pm 50^\circ$ is not active region open field, regardless of photospheric field strength.

Two examples of this categorization scheme are shown in the bottom two panels of Figure 1, with light colors representing coronal hole field lines and dark colors active region field lines.

3. Results

3.1. Location of Open Field Footpoints

The latitude (top panel) and longitude (bottom panel) distributions of active region open field footpoints across four solar cycles are shown in Figure 3. The longitude distributions

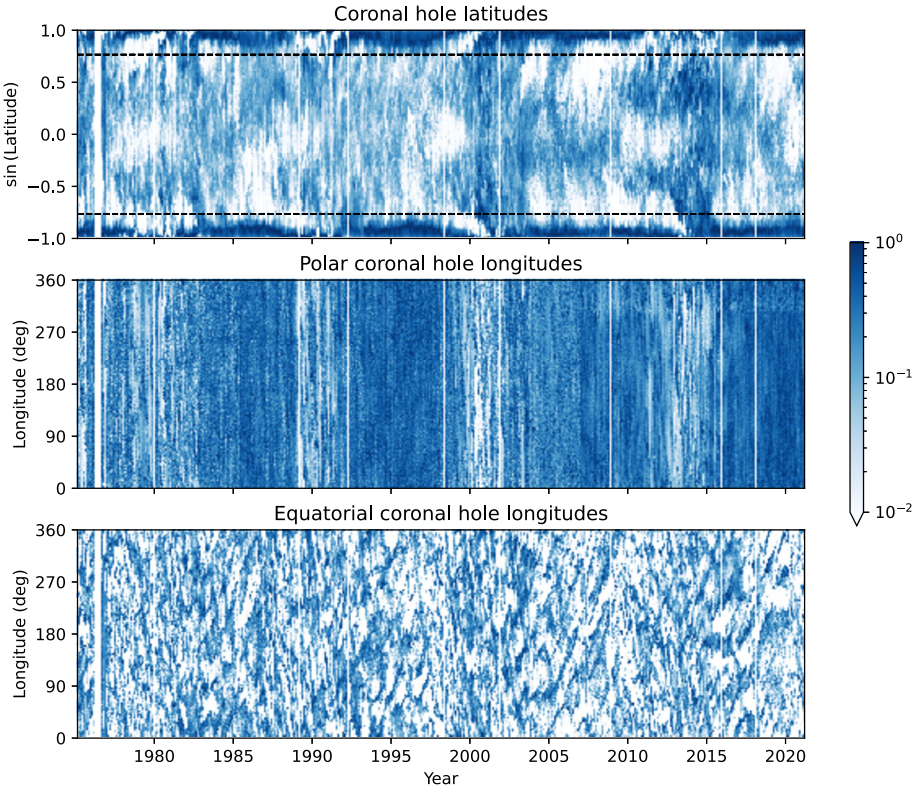

Figure 4 Distributions of open field solar surface footpoints in coronal holes as a function of time, column normalized. The top panel shows distributions as a function of sin(latitude) (summed over longitude), with horizontal black lines at $\pm 50°$. The middle panel shows the longitude distributions (summed over latitude) for polar coronal holes ($|\theta| > 50°$). The bottom panel shows the longitude distributions (summed over latitude) for low latitude coronal holes ($|\theta| < 50°$). Full datasets are used from KPVT and GONG, with the gap between filled by MDI.

reveal that AR sources are localized, typically lasting for only one or two solar rotations. A handful of regions lasted longer, and persisted for several rotations before their magnetic field dispersed to become weaker than the AR identification threshold. This agrees with observations of active region lifetimes (van Driel-Gesztelyi and Green, 2015), and we have manually checked some of the multiple-rotation trails in Figure 3 to verify that they match with active regions observable in EUV images over multiple rotations. The latitude distributions also agree with previous observations of active regions, notably the butterfly diagram that shows a reduction in active region latitudes as a solar cycle progresses (Carrington, 1858; Maunder, 1922).

The top panel of Figure 4 shows the latitude distribution of coronal hole open field footpoints. Recurring polar coronal holes are visible at high latitudes, alongside lower latitude equatorial coronal holes. Equatorial coronal holes exhibit a weak butterfly pattern, which is to be expected as they form from the diffusion of flux originally supplied by active region emergence. The middle panel of Figure 4 shows the longitude distribution of polar coronal hole open field footpoints, defined as footpoints at latitudes above $\pm 50°$. As expected there is little longitudinal structuring of the polar coronal holes, which for the majority of the solar

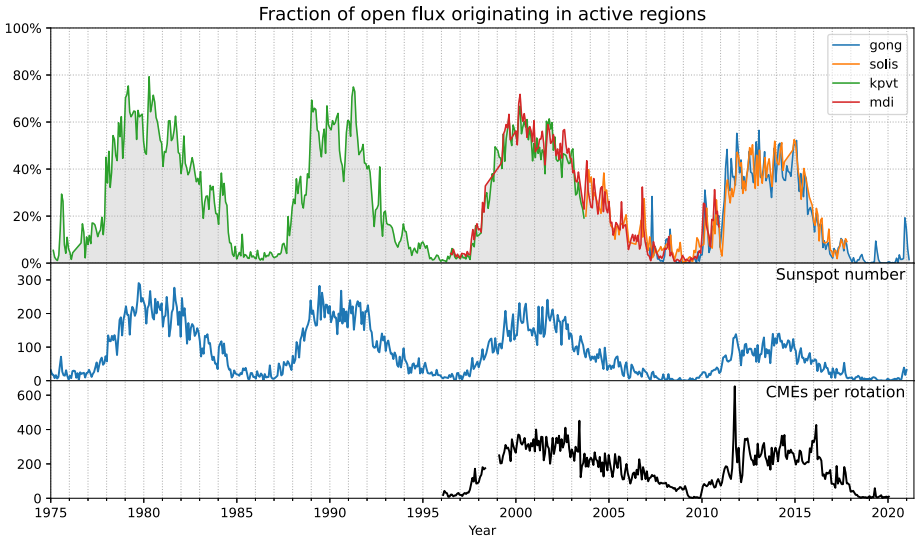

Figure 5 Fraction of open flux rooted in active regions as a function of time (top panel). Different observatories are denoted with different colors, as shown in the figure legend. The middle panel shows rotation-averaged sunspot number, and the bottom panel shows the number of CMEs per solar rotation taken from the LASCO CME catalogue.

cycle cover the entire poles. The bottom panel of Figure 4 shows the longitude distribution of equatorial coronal holes, i.e. latitudes below $\pm 50°$. As expected there is clear structuring in longitude, as equatorial coronal holes do not wrap all the way around the Sun. Several trails are evident in this figure, showing equatorial coronal holes that persist over multiple solar rotations. The drift of these trails in longitude with time is due to their rotation rate being slightly slower than the rotation rate used to define Carrington longitude. These trails agree with statistical results on the lifetimes of equatorial coronal holes, showing that they can exist for up to three years (Hewins et al., 2020).

Together the distributions of open field regions in active regions (Figure 3) and coronal holes (Figure 4), and their similarity to observational signatures of these features in EUV wavelengths give us confidence in our method for distinguishing between these two distinct solar wind source regions.

3.2. Contribution of Active Regions to the Solar Wind

The total open flux in each PFSS extrapolation was calculated by summing all radial magnetic field values on the source surface, and multiplying by the constant solid angle area element of each cell. The total open solar flux rooted in active regions was calculated the same way, but this time only summing over source surface pixels hosting an open field line with a photospheric footpoint rooted in an active region. The ratio of active region open flux to total open flux was taken as a proxy for their fractional contribution to all solar wind during a given solar rotation.

The fraction of total open flux rooted in active regions as a function of time is shown in the top panel of Figure 5. Results from different observatories are shown in different colored lines. Where they overlap, the results from each observatory agree well, even on monthly timescales within individual solar cycles. The fraction of open solar flux contained within

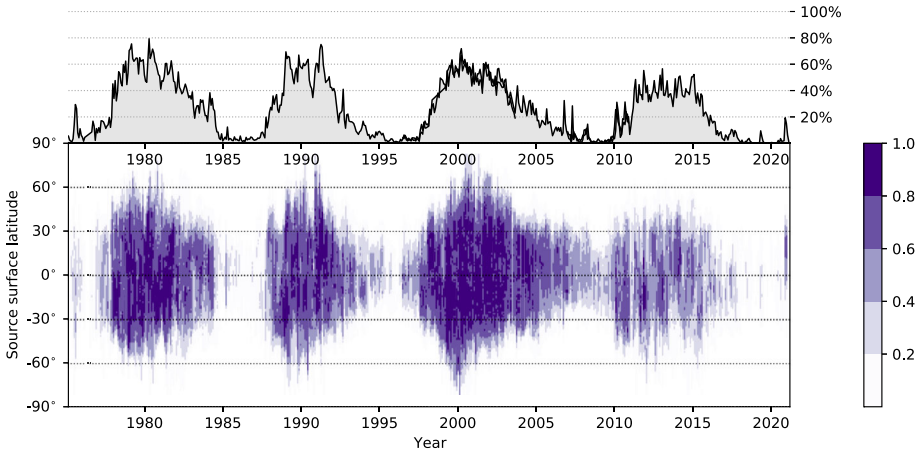

Figure 6 Fraction of open flux rooted in active regions as a function of source surface latitude and time, averaged over longitude. This is a proxy for solar wind latitude if solar wind propagation is radial beyond the source surface. The top panel shows the fraction averaged over all latitudes and longitudes, as previously shown in the top panel of Figure 5.

active regions follows the solar cycle; for comparison, the middle panel shows the rotation-averaged sunspot number (SILSO World Data Center, 2021). Larger amplitude sunspot cycles result in a larger fraction of open flux originating in active regions. This is a non-trivial result, depending on the details of how open flux is distributed between coronal holes (both equatorial and polar) and active regions, and how this varies with cycle amplitude. Even during the relatively weak maximum of Cycle 24, 40% – 50% of open flux originated in active regions, with even higher fractions during previous stronger maxima. This suggests that active regions play an equally important role to coronal holes as sources of the solar wind during solar maxima.

Because rearrangements in the global coronal magnetic field can be caused by coronal mass ejections (CMEs), the bottom panel of Figure 5 shows the CME rates over the last two solar cycles from the SOHO/LASCO CME catalogue (Gopalswamy et al., 2009). CMEs do not themselves contribute significantly to the solar wind mass flux (Mishra et al., 2019), but they could play a role in opening regions of previously closed magnetic flux within active regions. Although the correlation of active region open flux with CME rate is not as strong as with sunspot number, peaks in the CME rate (e.g. in 2003, 2011, 2016) appear to show a weak association with jumps in the amount of active region open flux. In addition, variations in active region open flux between individual solar rotations are typically 10% – 20%. This implies that the mechanism(s) significantly modifying the active region open flux are active on timescales shorter or equal to an individual solar rotation. This is consistent with CMEs being one mechanism driving these changes in the photospheric footpoints of open magnetic flux, but more investigation is needed to show if these are causal links.

As well as investigating variations over time, our dataset allows investigation of the angular extent of active region open flux in the heliosphere. Figure 6 shows the fraction of all source surface longitudes connected to active region open flux, as a function of source surface latitude and time. This reveals substantial variation between different solar cycles. During Cycles 21 – 23 active regions were connected to heliospheric latitudes $\pm 60°$, with their extent decreasing as the solar cycle declined. In contrast, during the Cycle 24 their heliospheric connections were typically limited to $\pm 30°$, with no obvious reduction in this

extent as the cycle progressed. The gaps during solar minima were also highly variable: between both Cycles 21, 22 and the current minima there were extended ~ 5 year periods with hardly any active region contributions to the solar wind, with a much shorter gap between Cycles 22, 23, and almost no gap between Cycles 23, 24.

4. Discussion

When discussing the origins of the solar wind, it is helpful to distinguish between source regions (e.g. coronal holes, active regions) and release mechanisms (e.g. long-term open flux, interchange reconnection, closed-flux reconnection); see Viall and Borovsky (2020) Section 2.1 for a thorough discussion of this distinction. In this paper we have used PFSS models to understand the balance of source regions between coronal holes and active regions, and how this evolves over the solar cycle (see Figure 5), but have not addressed different release mechanisms. There are several studies investigating possible release mechanisms of solar wind within individual active regions (e.g. Baker, van Driel-Gesztelyi, and Attrill, 2007; van Driel-Gesztelyi et al., 2012; Brooks et al., 2020). Understanding if these mechanisms are universal properties of all active region sources combined with our new analysis of the prevalence of active region sources gives a route to understanding how solar wind release mechanisms vary over the solar cycle. In addition it should be possible to combine this information with in-situ diagnostics for solar wind origin (e.g. Baker et al., 2009; Stansby, Horbury, and Matteini, 2019; Owens et al., 2020) to further understand how similar or different release mechanisms are in different active regions.

A potential source of error in modeling multiple solar cycles is the necessary inclusion of magnetograms measured by a range of different observatories that are not fully intercalibrated (e.g. Jones and Ceja, 2001; Tran et al., 2005; Demidov et al., 2008; Pietarila et al., 2013; Riley et al., 2014). We have mitigated against these differences by choosing observatory specific thresholds for identifying active region open flux (Table 1). Although some inconsistency in the fraction of active region open flux is inevitable and present, there is agreement almost always to within $\pm 10\%$ between different observatories when they were observing together (Figure 5).

Changing the source surface radius in PFSS models can modify the exact photospheric locations of open flux, but we have shown that the fraction of open flux rooted in ARs is insensitive to this parameter, within a range of reasonable values (Figure 7). In contrast, varying R_{ss} causes significant variation in the global distribution and location of coronal hole open flux, meaning we could not accurately distinguish between equatorial and polar coronal holes. Further work combining our methodology with EUV observations of coronal holes (e.g. Hess Webber et al., 2014; Hewins et al., 2020) to constrain R_{ss} could be used to remove this limitation.

We have hypothesized that the mechanism opening up new active region open flux is interchange reconnection in the corona. There is evidence that this coronal process can occur gradually and continuously (e.g. Higginson et al., 2017), or as more discrete CME events (e.g. Cohen et al., 2009; van Driel-Gesztelyi et al., 2014), but it is not clear which of these processes dominates on a global scale. It is not possible to directly investigate this question within PFSS models, which are time-independent snapshots of the coronal field. Time evolving magnetofrictional simulations could be used, however, where the boundary photospheric magnetic field is evolved in time to drive coronal magnetic field evolution (Yeates, 2014). These models have previously been used to predict where flux ropes form and erupt in the corona (Yeates, 2014; Lowder and Yeates, 2017), but it should also be possible to identify interchange reconnection occurring in these simulations, giving a possible avenue into investigating the mechanisms behind the opening and closing of active region open flux.

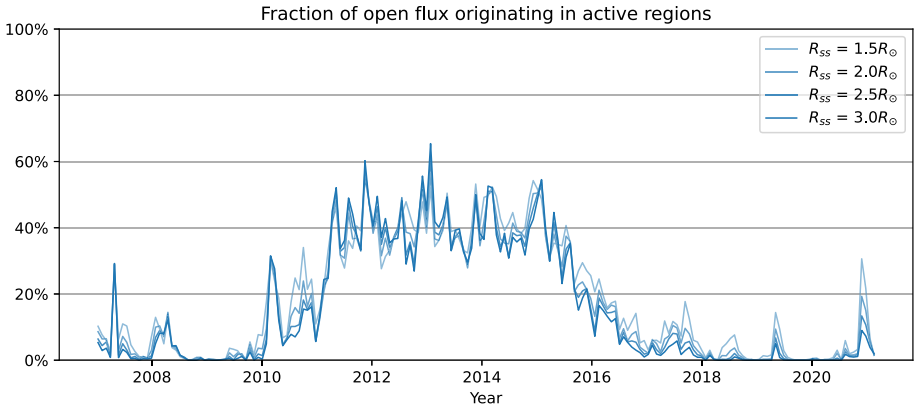

Figure 7 The effect of varying R_{ss} on estimates of the fraction of open flux rooted in active regions. All data are from GONG, with different R_{ss} values indicated by different line weights from light (low R_{ss}) to dark (high R_{ss}).

The fraction of solar wind originating in active regions could have implications for the properties of the solar wind, and how this affects the heliosphere across the solar cycle. Backmapping solar wind measured at 1 AU to active region sources identified in EUV images shows that active region solar wind is slower than the average solar wind (Fu et al., 2015; Zhao et al., 2017). Active regions are hotter than coronal holes, which drives increased mass fluxes in the corona (Stansby et al., 2020b), but in the case of the Sun the magnetic field expansion almost exactly cancels this difference out, resulting in a remarkably constant solar wind mass flux (Wang, 2010) that is independent of source type. There is still plenty of scope for further investigation of the properties of solar wind originating in active regions. When coupled with our results on the time-latitude distribution of active region sources (Figure 6) this could provide a way to predict heliospheric conditions where active region solar wind dominates.

5. Conclusions

Using global potential field source surface modeling of the corona (Section 2), we have estimated what fraction of solar wind originates in active regions, as a function of latitude and time. The fractional contribution of active regions to the solar wind is negligible at solar minimum, and typically 40% – 60% at solar maximum, scaling with sunspot number (Figure 5). The latitudinal extent of active region solar wind is highly variable between different solar cycles (Figure 6): in Cycles 21 – 23 active region wind extended to $\pm 60°$, but during the weaker Cycle 24 typically only reached $\pm 30°$. Even if the upcoming Cycle 25 is a weak cycle, Parker Solar Probe (Fox et al., 2016) and Solar Orbiter (Müller et al., 2020) will observe an increasing amount of solar wind from active region sources, allowing further understanding of the properties and release mechanisms of active region solar wind.

Appendix: Varying Source Surface Radius

To check that the results in Figure 5 are not affected by model parameters, Figure 7 shows the fraction of open flux originating in active regions for PFSS model source surface heights

ranging from 1.5 $R_\odot$ (thinnest line) to 3.0 $R_\odot$ (thickest line). While for some rotations there is a slight tendency for smaller source surface radii to result in a slightly larger fraction of flux rooted in active regions, this is a small effect and does not change any of the conclusions in this paper.

Acknowledgements D.S. is supported by STFC grant ST/S000240/1. L.v.D.G. is partially funded under STFC consolidated grant number ST/S000240/1 and acknowledges the Hungarian National Research, Development and Innovation Office grant OTKA K-131508. L. M. G. is grateful to the Royal Society for support through a University Research Fellowship. T. S. H. is supported by STFC grant ST/S000364/1. The authors thank the referee for constructive comments that improved the paper. This research used the following software packages: pfsspy (Stansby, Yeates, and Badman, 2020), sunpy (The SunPy Community et al., 2020), astropy (The Astropy Collaboration et al., 2018), Matplotlib (Hunter, 2007). This work utilizes SOLIS data obtained by the NSO Integrated Synoptic Program (NISP), managed by the National Solar Observatory, which is operated by the Association of Universities for Research in Astronomy (AURA), Inc. under a cooperative agreement with the National Science Foundation. NSO/Kitt Peak data used here are produced cooperatively by NSF/NOAO, NASA/GSFC, and NOAA/SEL. This work utilizes data from the National Solar Observatory Integrated Synoptic Program, which is operated by the Association of Universities for Research in Astronomy, under a cooperative agreement with the National Science Foundation and with additional financial support from the National Oceanic and Atmospheric Administration, the National Aeronautics and Space Administration, and the United States Air Force. The GONG network of instruments is hosted by the Big Bear Solar Observatory, High Altitude Observatory, Learmonth Solar Observatory, Udaipur Solar Observatory, Instituto de Astrofísica de Canarias, and Cerro Tololo Interamerican Observatory. SOHO is a project of international cooperation between ESA and NASA. This CME catalog is generated and maintained at the CDAW Data Center by NASA and The Catholic University of America in cooperation with the Naval Research Laboratory.

Declarations

Declaration of Potential Conflicts of Interest The authors declare that they have no conflicts of interest.

Open Access This article is licensed under a Creative Commons Attribution 4.0 International License, which permits use, sharing, adaptation, distribution and reproduction in any medium or format, as long as you give appropriate credit to the original author(s) and the source, provide a link to the Creative Commons licence, and indicate if changes were made. The images or other third party material in this article are included in the article's Creative Commons licence, unless indicated otherwise in a credit line to the material. If material is not included in the article's Creative Commons licence and your intended use is not permitted by statutory regulation or exceeds the permitted use, you will need to obtain permission directly from the copyright holder. To view a copy of this licence, visit http://creativecommons.org/licenses/by/4.0/.

References

Altschuler, M.D., Newkirk, G.: 1969, Magnetic fields and the structure of the solar corona. *Solar Phys.* **9**, 131. DOI.

Arden, W.M., Norton, A.A., Sun, X.: 2014, A "breathing" source surface for cycles 23 and 24. *J. Geophys. Res. Space Phys.* **119**, 1476. DOI.

Asvestari, E., Heinemann, S.G., Temmer, M., Pomoell, J., Kilpua, E., Magdalenic, J., Poedts, S.: 2019, Reconstructing coronal hole areas with EUHFORIA and adapted WSA model: optimizing the model parameters. *J. Geophys. Res. Space Phys.* **124**, 8280. DOI.

Attrill, G., Nakwacki, M.S., Harra, L.K., Van Driel-Gesztelyi, L., Mandrini, C.H., Dasso, S., Wang, J.: 2006, Using the evolution of coronal dimming regions to probe the global magnetic field topology. *Solar Phys.* **238**, 117. DOI.

Badman, S.T., Bale, S.D., Oliveros, J.C.M., Panasenco, O., Velli, M., Stansby, D., Buitrago-Casas, J.C., Réville, V., Bonnell, J.W., Case, A.W., de Wit, T.D., Goetz, K., Harvey, P.R., Kasper, J.C., Korreck, K.E., Larson, D.E., Livi, R., MacDowall, R.J., Malaspina, D.M., Pulupa, M., Stevens, M.L., Whittlesey, P.L.: 2020, Magnetic connectivity of the ecliptic plane within 0.5 au: potential field source surface modeling of the first Parker Solar Probe encounter. *Astrophys. J. Suppl.* **246**, 23. DOI.

Baker, D., van Driel-Gesztelyi, L., Attrill, G.D.R.: 2007, Evidence for interchange reconnection between a coronal hole and an adjacent emerging flux region. *Astron. Nachr.* **328**, 773. DOI.

Baker, D., Rouillard, A.P., van Driel-Gesztelyi, L., Démoulin, P., Harra, L.K., Lavraud, B., Davies, J.A., Opitz, A., Luhmann, J.G., Sauvaud, J.-A., Galvin, A.B.: 2009, Signatures of interchange reconnection: STEREO, ACE and Hinode observations combined. *Ann. Geophys.* **27**, 3883. DOI.

The SunPy Community, Barnes, a.W.T., Bobra, M.G., Christe, S.D., Freij, N., Hayes, L.A., Ireland, J., Mumford, S., Perez-Suarez, D., Ryan, D.F., Shih, A.Y., Chanda, P., Glogowski, K., Hewett, R., Hughitt, V.K., Hill, A., Hiware, K., Inglis, A., Kirk, M.S.F., Konge, S., Mason, J.P., Maloney, S.A., Murray, S.A., Panda, A., Park, J., Pereira, T.M.D., Reardon, K., Savage, S., Sip\Hocz, B.M., Stansby, D., Jain, Y., Taylor, G., Yadav, T., Rajul, Dang, T.K.: 2020, The SunPy project: open source development and status of the version 1.0 Core package. *Astrophys. J.* **890**, 68. DOI.

Brooks, D.H., Winebarger, A.R., Savage, S., Warren, H.P., Pontieu, B.D., Peter, H., Cirtain, J.W., Golub, L., Kobayashi, K., McIntosh, S.W., McKenzie, D., Morton, R., Rachmeler, L., Testa, P., Tiwari, S., Walsh, R.: 2020, The drivers of active region outflows into the slow solar wind. *Astrophys. J.* **894**, 144. DOI.

Carrington, R.C.: 1858, On the distribution of the solar spots in latitudes since the beginning of the year 1854, with a map. *Mon. Not. Roy. Astron. Soc.* **19**, 1. DOI.

Cheung, M.C.M., van Driel-Gesztelyi, L., Martínez Pillet, V., Thompson, M.J.: 2017, The life cycle of active region magnetic fields. *Space Sci. Rev.* **210**, 317. DOI.

Clark, R., Harvey, J., Hill, F., Toner, C.: 2003, GONG Magnetogram Zero-Point Correction Status **34**, 08.03. ADS.

Cohen, O., Attrill, G.D.R., Manchester, W.B. IV, Wills-Davey, M.J.: 2009, Numerical simulation of an EUV coronal wave based on the 2009 February 13 CME event observed by STEREO. *Astrophys. J.* **705**, 587. DOI.

Demidov, M.L., Golubeva, E.M., Balthasar, H., Staude, J., Grigoryev, V.M.: 2008, Comparison of solar magnetic fields measured at different observatories: peculiar strength ratio distributions across the disk. *Solar Phys.* **250**, 279. DOI.

Fox, N.J., Velli, M.C., Bale, S.D., Decker, R., Driesman, A., Howard, R.A., Kasper, J.C., Kinnison, J., Kusterer, M., Lario, D., Lockwood, M.K., McComas, D.J., Raouafi, N.E., Szabo, A.: 2016, The Solar Probe Plus mission: humanity's first visit to our star. *Space Sci. Rev.* **204**, 7. DOI.

Fu, H., Li, B., Li, X., Huang, Z., Mou, C., Jiao, F., Xia, L.: 2015, Coronal sources and in situ properties of the solar winds sampled by ACE during 1999 – 2008. *Solar Phys.* **290**, 1399. DOI.

Golubeva, E.M., Mordvinov, A.V.: 2017, Rearrangements of open magnetic flux and formation of polar coronal holes in cycle 24. *Solar Phys.* **292**, 175. DOI.

Gopalswamy, N., Yashiro, S., Michalek, G., Stenborg, G., Vourlidas, A., Freeland, S., Howard, R.: 2009, The SOHO/LASCO CME catalog. *Earth Moon Planets* **104**, 295. DOI.

Harvey, J.W., Hill, F., Hubbard, R.P., Kennedy, J.R., Leibacher, J.W., Pintar, J.A., Gilman, P.A., Noyes, R.W., Title, A.M., Toomre, J., Ulrich, R.K., Bhatnagar, A., Kennewell, J.A., Marquette, W., Patrón, J., Saá, O., Yasukawa, E.: 1996, The Global Oscillation Network Group (GONG) project. *Science* **272**, 1284. Chap. Articles. DOI.

Harvey, J., Giampapa, M., Henney, C., Jones, H., Keller, C.: 2003, First results from SOLIS. *AGU Fall Meet. Abstr.* **42**, SH42B. ADS.

Hess Webber, S.A., Karna, N., Pesnell, W.D., Kirk, M.S.: 2014, Areas of polar coronal holes from 1996 through 2010. *Solar Phys.* **289**, 4047. DOI.

Hewins, I.M., Gibson, S.E., Webb, D.F., McFadden, R.H., Kuchar, T.A., Emery, B.A., McIntosh, S.W.: 2020, The evolution of coronal holes over three solar cycles using the McIntosh archive. *Solar Phys.* **295**, 161. DOI.

Higginson, A.K., Antiochos, S.K., DeVore, C.R., Wyper, P.F., Zurbuchen, T.H.: 2017, Dynamics of coronal hole boundaries. *Astrophys. J.* **837**, 113. DOI.

Hoeksema, J.T., Wilcox, J.M., Scherrer, P.H.: 1983, The structure of the heliospheric current sheet: 1978 – 1982. *J. Geophys. Res. Space Phys.* **88**, 9910. DOI.

Hunter, J.D.: 2007, Matplotlib: a 2D graphics environment. *Comput. Sci. Eng.* **9**, 90. DOI.

Jones, H.P., Ceja, J.A.: 2001, Preliminary comparison of magnetograms from KPVT/SPM, SOHO/MDI and GONG$^+$. In: Sigwarth, M. (ed.) *Advanced Solar Polarimetry – Theory, Observation, and Instrumentation*, *Astronomical Society of the Pacific Conference Series* **236**, 87. ADS.

Keller, C.U., NSO Staff: 1998, SOLIS—a modern facility for synoptic solar observations. **154**, 636. ADS.

Kong, D.F., Pan, G.M., Yan, X.L., Wang, J.C., Li, Q.L.: 2018, Observational evidence of interchange reconnection between a solar coronal hole and a small emerging active region. *Astrophys. J.* **863**, L22. DOI.

Lee, C.O., Luhmann, J.G., Hoeksema, J.T., Sun, X., Arge, C.N., de Pater, I.: 2011, Coronal field opens at lower height during the solar cycles 22 and 23 minimum periods: IMF comparison suggests the source surface should be lowered. *Solar Phys.* **269**, 367. DOI.

Leighton, R.B.: 1964, Transport of magnetic fields on the Sun. *Astrophys. J.* **140**, 1547. DOI.
Liu, Y., Hoeksema, J.T., Scherrer, P.H., Schou, J., Couvidat, S., Bush, R.I., Duvall, T.L., Hayashi, K., Sun, X., Zhao, X.: 2012, Comparison of line-of-sight magnetograms taken by the Solar Dynamics Observatory/Helioseismic and Magnetic Imager and Solar and Heliospheric Observatory/Michelson Doppler Imager. *Solar Phys.* **279**, 295. DOI.
Livingston, W.C., Harvey, J., Pierce, A.K., Schrage, D., Gillespie, B., Simmons, J., Slaughter, C.: 1976, Kitt peak 60-cm vacuum telescope. *Appl. Opt.* **15**, 33. DOI.
Lockwood, M., Owens, M.: 2009, The accuracy of using the Ulysses result of the spatial invariance of the radial heliospheric field to compute the open solar flux. *Astrophys. J.* **701**, 964. DOI.
Lowder, C., Yeates, A.: 2017, Magnetic flux rope identification and characterization from observationally driven solar coronal models. *Astrophys. J.* **846**, 106. DOI.
Ma, L., Qu, Z.-Q., Yan, X.-L., Xue, Z.-K.: 2014, Interchange reconnection between an active region and a coronal hole. *Res. Astron. Astrophys.* **14**, 221. DOI.
Macneil, A.R., Owen, C.J., Baker, D., Brooks, D.H., Harra, L.K., Long, D.M., Wicks, R.T.: 2019, Active region modulation of coronal hole solar wind. *Astrophys. J.* **887**, 146. DOI.
Maunder, E.W.: 1922, The Sun and sun-spots, 1820 – 1920. *Mon. Not. Roy. Astron. Soc.* **82**, 534. DOI.
McComas, D.J., Angold, N., Elliott, H.A., Livadiotis, G., Schwadron, N.A., Skoug, R.M., Smith, C.W.: 2013, Weakest solar wind of the space age and the current "mini" solar maximum. *Astrophys. J.* **779**, 2. DOI.
Mishra, W., Srivastava, N., Wang, Y., Mirtoshev, Z., Zhang, J., Liu, R.: 2019, Mass loss via solar wind and coronal mass ejections during solar cycles 23 and 24. *Mon. Not. Roy. Astron. Soc.* **486**, 4671. DOI.
Müller, D., Cyr, O.C.S., Zouganelis, I., Gilbert, H.R., Marsden, R., Nieves-Chinchilla, T., Antonucci, E., Auchère, F., Berghmans, D., Horbury, T.S., Howard, R.A., Krucker, S., Maksimovic, M., Owen, C.J., Rochus, P., Rodriguez-Pacheco, J., Romoli, M., Solanki, S.K., Bruno, R., Carlsson, M., Fludra, A., Harra, L., Hassler, D.M., Livi, S., Louarn, P., Peter, H., Schühle, U., Teriaca, L., Iniesta, J.C.d.T., Wimmer-Schweingruber, R.F., Marsch, E., Velli, M., Groof, A.D., Walsh, A., Williams, D.: 2020, The Solar Orbiter mission - science overview. *Astron. Astrophys.* **642**, A1. DOI.
Neugebauer, M., Liewer, P.C., Smith, E.J., Skoug, R.M., Zurbuchen, T.H.: 2002, Sources of the solar wind at solar activity maximum. *J. Geophys. Res. Space Phys.* **107**, SSH 13. DOI.
Owens, M., Lockwood, M., Macneil, A., Stansby, D.: 2020, Signatures of coronal loop opening via interchange reconnection in the slow solar wind at 1 AU. *Solar Phys.* **295**, 37. DOI.
Petrie, G.J.D., Haislmaier, K.J.: 2013, Low-latitude coronal holes, decaying active regions, and global coronal magnetic structure. *Astrophys. J.* **775**, 100. DOI.
Pietarila, A., Bertello, L., Harvey, J.W., Pevtsov, A.A.: 2013, Comparison of ground-based and space-based longitudinal magnetograms. *Solar Phys.* **282**, 91. DOI.
The Astropy Collaboration, Price-Whelan, A.M., Sipőcz, B.M., Günther, H.M., Lim, P.L., Crawford, S.M., Conseil, S., Shupe, D.L., Craig, M.W., Dencheva, N., Ginsburg, A., VanderPlas, J.T., Bradley, L.D., Pérez-Suárez, D., de Val-Borro, M., Aldcroft, T.L., Cruz, K.L., Robitaille, T.P., Tollerud, E.J., Ardelean, C., Babej, T., Bach, Y.P., Bachetti, M., Bakanov, A.V., Bamford, S.P., Barentsen, G., Barmby, P., Baumbach, A., Berry, K.L., Biscani, F., Boquien, M., Bostroem, K.A., Bouma, L.G., Brammer, G.B., Bray, E.M., Breytenbach, H., Buddelmeijer, H., Burke, D.J., Calderone, G., Rodríguez, J.L.C., Cara, M., Cardoso, J.V.M., Cheedella, S., Copin, Y., Corrales, L., Crichton, D., D'Avella, D., Deil, C., Depagne, É., Dietrich, J.P., Donath, A., Droettboom, M., Earl, N., Erben, T., Fabbro, S., Ferreira, L.A., Finethy, T., Fox, R.T., Garrison, L.H., Gibbons, S.L.J., Goldstein, D.A., Gommers, R., Greco, J.P., Greenfield, P., Groener, A.M., Grollier, F., Hagen, A., Hirst, P., Homeier, D., Horton, A.J., Hosseinzadeh, G., Hu, L., Hunkeler, J.S., Ivezić, Ž., Jain, A., Jenness, T., Kanarek, G., Kendrew, S., Kern, N.S., Kerzendorf, W.E., Khvalko, A., King, J., Kirkby, D., Kulkarni, A.M., Kumar, A., Lee, A., Lenz, D., Littlefair, S.P., Ma, Z., Macleod, D.M., Mastropietro, M., McCully, C., Montagnac, S., Morris, B.M., Mueller, M., Mumford, S.J., Muna, D., Murphy, N.A., Nelson, S., Nguyen, G.H., Ninan, J.P., Nöthe, M., Ogaz, S., Oh, S., Parejko, J.K., Parley, N., Pascual, S., Patil, R., Patil, A.A., Plunkett, A.L., Prochaska, J.X., Rastogi, T., Janga, V.R., Sabater, J., Sakurikar, P., Seifert, M., Sherbert, L.E., Sherwood-Taylor, H., Shih, A.Y., Sick, J., Silbiger, M.T., Singanamalla, S., Singer, L.P., Sladen, P.H., Sooley, K.A., Sornarajah, S., Streicher, O., Teuben, P., Thomas, S.W., Tremblay, G.R., Turner, J.E.H., Terrón, V., van Kerkwijk, M.H., de la Vega, A., Watkins, L.L., Weaver, B.A., Whitmore, J.B., Woillez, J., Zabalza, V.: 2018, The Astropy project: building an open-science project and status of the v2.0 Core package. *Astron. J.* **156**, 123. DOI.
Riley, P., Ben-Nun, M., Linker, J.A., Mikic, Z., Svalgaard, L., Harvey, J., Bertello, L., Hoeksema, T., Liu, Y., Ulrich, R.: 2014, A multi-observatory inter-comparison of line-of-sight synoptic solar magnetograms. *Solar Phys.* **289**, 769. DOI.
Schatten, K.H., Wilcox, J.M., Ness, N.F.: 1969, A model of interplanetary and coronal magnetic fields. *Solar Phys.* **6**, 442. DOI.
Scherrer, P.H., Bogart, R.S., Bush, R.I., Hoeksema, J.T., Kosovichev, A.G., Schou, J., Rosenberg, W., Springer, L., Tarbell, T.D., Title, A., Wolfson, C.J., Zayer, I., MDI Engineering Team: 1995, The solar oscillations investigation - Michelson Doppler Imager. *Solar Phys.* **162**, 129. DOI.

Schrijver, C.J., De Rosa, M.L.: 2003, Photospheric and heliospheric magnetic fields. *Solar Phys.* **212**, 165. DOI.
Sheeley, N.R., Wang, Y.-M., Harvey, J.W.: 1989, The effect of newly erupting flux on the polar coronal holes. *Solar Phys.* **119**, 323. DOI.
SILSO World Data Center: 2021, *The International Sunspot Number*, Royal Observatory of Belgium, avenue Circulaire 3, 1180 Brussels, Belgium. http://www.sidc.be/silso/.
Stansby, D., Horbury, T.S., Matteini, L.: 2019, Diagnosing solar wind origins using in situ measurements in the inner heliosphere. *Mon. Not. Roy. Astron. Soc.* **482**, 1706. DOI.
Stansby, D., Yeates, A., Badman, S.T.: 2020, Pfsspy: a Python package for potential field source surface modelling. *J. Open Sour. Softw.* **5**, 2732. DOI.
Stansby, D., Baker, D., Brooks, D.H., Owen, C.J.: 2020a, Directly comparing coronal and solar wind elemental fractionation. *Astron. Astrophys.* **640**, A28. DOI.
Stansby, D., Berčič, L., Matteini, L., Owen, C.J., French, R., Baker, D., Badman, S.T.: 2020b, Sensitivity of solar wind mass flux to coronal temperature. *Astron. Astrophys.*. DOI.
Tian, H., Harra, L., Baker, D., Brooks, D.H., Xia, L.: 2021, Upflows in the upper solar atmosphere. *Solar Phys.* **296**, 47. DOI.
Tran, T., Bertello, L., Ulrich, R.K., Evans, S.: 2005, Magnetic fields from SOHO MDI converted to the Mount Wilson 150 Foot Solar tower scale. *Astrophys. J. Suppl.* **156**, 295. DOI.
van Driel-Gesztelyi, L., Green, L.M.: 2015, Evolution of active regions. *Living Rev. Solar Phys.* **12**, 1. DOI.
van Driel-Gesztelyi, L., Culhane, J.L., Baker, D., Démoulin, P., Mandrini, C.H., DeRosa, M.L., Rouillard, A.P., Opitz, A., Stenborg, G., Vourlidas, A., Brooks, D.H.: 2012, Magnetic topology of active regions and coronal holes: implications for coronal outflows and the solar wind. *Solar Phys.* **281**, 237. DOI.
van Driel-Gesztelyi, L., Baker, D., Török, T., Pariat, E., Green, L.M., Williams, D.R., Carlyle, J., Valori, G., Démoulin, P., Kliem, B., Long, D.M., Matthews, S.A., Malherbe, J.-M.: 2014, Coronal magnetic reconnection driven by CME expansion—the 2011 June 7 event. *Astrophys. J.* **788**, 85. DOI.
Viall, N.M., Borovsky, J.E.: 2020, Nine outstanding questions of solar wind physics. *J. Geophys. Res. Space Phys.* **125**, e2018JA026005. DOI.
Virtanen, I.I., Koskela, J.S., Mursula, K.: 2020, Abrupt shrinking of solar corona in the late 1990s. *Astrophys. J.* **889**, L28. DOI.
Virtanen, I., Mursula, K.: 2017, Photospheric and coronal magnetic fields in six magnetographs - II. Harmonic scaling of field intensities. *Astron. Astrophys.* **604**, A7. DOI.
Virtanen, I.O.I., Virtanen, I.I., Pevtsov, A.A., Yeates, A., Mursula, K.: 2017, Reconstructing solar magnetic fields from historical observations - II. Testing the surface flux transport model. *Astron. Astrophys.* **604**, A8. DOI.
Wang, Y.-M.: 2010, On the relative constancy of the solar wind mass flux at 1 Au. *Astrophys. J.* **715**, L121. DOI.
Wang, Y.-M.: 2017, Small coronal holes near active regions as sources of slow solar wind. *Astrophys. J.* **841**, 94. DOI.
Wang, Y.-M., Sheeley, J.N.R.: 2003a, On the topological evolution of the coronal magnetic field during the solar cycle. *Astrophys. J.* **599**, 1404. DOI.
Wang, Y.-M., Sheeley, J.N.R.: 2003b, The solar wind and its magnetic sources at sunspot maximum. *Astrophys. J.* **587**, 818. DOI.
Wang, Y.-M., Robbrecht, E., Rouillard, A.P., Sheeley, N.R., Thernisien, A.F.R.: 2010, Formation and evolution of coronal holes following the emergence of active regions. *Astrophys. J.* **715**, 39. DOI.
Wenzler, T., Solanki, S.K., Krivova, N.A., Fluri, D.M.: 2004, Comparison between KPVT/SPM and SoHO/MDI magnetograms with an application to solar irradiance reconstructions. *Astron. Astrophys.* **427**, 1031. DOI.
Whitbread, T., Yeates, A.R., Muñoz-Jaramillo, A., Petrie, G.J.D.: 2017, Parameter optimization for surface flux transport models. *Astron. Astrophys.* **607**, A76. DOI.
Yeates, A.R.: 2014, Coronal magnetic field evolution from 1996 to 2012: continuous non-potential simulations. *Solar Phys.* **289**, 631. DOI.
Yeates, A.R., Baker, D., van Driel-Gesztelyi, L.: 2015, Source of a prominent poleward surge during solar cycle 24. *Solar Phys.* **290**, 3189. DOI.
Zhao, L., Landi, E., Lepri, S.T., Gilbert, J.A., Zurbuchen, T.H., Fisk, L.A., Raines, J.M.: 2017, On the relation between the in situ properties and the coronal sources of the solar wind. *Astrophys. J.* **846**, 135. DOI.

Publisher's Note Springer Nature remains neutral with regard to jurisdictional claims in published maps and institutional affiliations.